JOURNAL OF PROPULSION AND POWER
Vol. 17, No. 1, January–February 2001

Erosion Resistance of Carbon–Carbon Ion Optics

J. S. Meserole*
The Boeing Company, Seattle, Washington 98124

A principal consideration in the design of ion thrusters for spacecraft propulsion is erosion of the downstream grid in the ion optics. Achieving adequate lifetime (10,000 h or more for many potential missions) without grid wear-through can impose significant constraints on thruster performance. The conventional material for making ion thruster grids is molybdenum. It is predicted that the wear rate of grids made of carbon–carbon composite should be one-eighth to one-ninth that of molybdenum grids. A pair of tests of carbon–carbon and molybdenum grids were conducted under nearly identical operating conditions to determine if carbon–carbon would exhibit the expected resistance to erosion. The result matched the prediction. Some uncertainty in the data, however, precluded a fully definitive verification. Also, a procedural investigation showed that presence of oxygen, water vapor, and nitrogen greatly increases the carbon–carbon erosion rate.

Introduction

FOR planetary exploration missions and for some Earth-orbit applications, ion propulsion offers substantial benefits in reduced spacecraft mass. Because ion thrusters produce very low thrust, they must operate for thousands of hours. Flight qualification of an ion thruster requires demonstrating a lifetime of 5,000–10,000 h or more. For most missions of current interest, the principal life-limiting element in an ion propulsion system is the thruster ion optics; that is, the grids that accelerate the ions to produce thrust.[1,2] In a two-grid optics set, the accelerator grid is steadily eroded by the impact of charge-exchange ions produced just beyond the grid and drawn back to it by its negative potential.[3–7] In life tests conducted in vacuum chambers, erosion is accelerated because the xenon background pressure near the thruster is higher than in space, which results in greater production of charge-exchange ions.[8]

The standard material used for making ion thruster grids is molybdenum. Of the refractory metals, this has the best combination of mechanical properties and low sputter yield. Tests have demonstrated, however, that to operate molybdenum grids for more than a few thousand hours requires that the thruster be throttled far below the maximum beam current density, or thrust density, that the thruster is physically capable of. This is because the erosion rate increases with beam density. A way to alleviate this constraint on thruster performance promises to be the use of grids made of carbon fiber/carbon matrix composite material.

The advantages of carbon–carbon grids are that carbon erodes much slower under ion impact than molybdenum does, and carbon–carbon composite has a near-zero coefficient of thermal expansion. The thermomechanical stability of carbon–carbon grids will enable closer grid spacing in large thrusters. This produces a higher maximum beam density than has previously been possible, and the high resistance to grid erosion enables long grid life under continuous operation at high beam density.

The first investigation of carbon ion thruster grids was a test in 1963 of flat graphite grids.[9] The objective was a solution to the problem of thermal distortion of molybdenum grids, and although the performance of the graphite grids was similar to that of molybdenum grids, the flexibility and relative fragility of the graphite were serious drawbacks. Today, graphite grids are used in commercial ion beam sources for industrial applications, where requirements for performance and tolerance to vibration are not so demanding as they are for spacecraft. Monheiser and Wilbur[10] conducted comparative 50-h erosion tests of small graphite and molybdenum grids. Depth measurements of the eroded areas indicated that the molybdenum eroded several times faster than the graphite, but the amount of erosion of the graphite was too little to provide a more definitive determination of the relative erosion rates. Garner and Brophy[11] subjected carbon and molybdenum badges to erosion tests within an ion thruster discharge chamber. In that environment, the carbon eroded only 25% less than the molybdenum. They concluded that contamination by oxygen and nitrogen was likely responsible for this anomalous result. Garner and Brophy also made 15-cm carbon–carbon grids and demonstrated that they functioned equally as well as molybdenum grids, but they did not operate the grids for enough time to determine the erosion rate.[12] Subsequent to the erosion testing reported herein, Mueller et al.[13] conducted a 700-h wear test of three-grid carbon–carbon ion optics. No erosion of either the accelerator or decelerator grids was evident, but both were at the relatively low potential of 100 V, which is just the threshold at which xenon ions begin to sputter carbon at all.

Hedges and Meserole[14] previously conducted comparative tests of carbon–carbon and molybdenum grid sets and demonstrated similar thruster operation with the two types. Further testing to compare the erosion resistances of the two accelerator grids yielded an unexpectedly high carbon erosion rate: one-third as much as with molybdenum.[15] The background pressure in the test chamber during these tests was kept relatively high, about 2×10^{-3} Pa, to accelerate the erosion. Also, the test setup unintentionally caused the background pressure to be 50% higher for the carbon–carbon test than for the molybdenum test. Later, a repeat test of the carbon–carbon gridset at the same background pressure as in the molybdenum test resulted in as much erosion of the accelerator grid as in the initial test.

The purpose of the tests described in the present paper was twofold: to demonstrate, if possible, the near order-of-magnitude reduction in erosion rate anticipated with carbon grids and to identify the reason for the unexpected carbon erosion in the previous tests. The initial report of this work[16] concluded that the carbon–carbon eroded much less than anticipated, but further analysis for this paper identified and corrected for an aspect of the testing that had biased the earlier analysis.

Ion Optics Description

The 10-cm-diam carbon and molybdenum grid sets used in the tests were fabricated to be as similar as possible. The only notable difference is that the molybdenum grids had to be dished, and the carbon grids were made flat. That the latter could be flat is an advantage conferred by the small coefficient of thermal expansion of carbon–carbon composite material. The number of holes, their sizes,

Presented as Paper 94-3119 at the AIAA/ASME/SAE/ASEE 30th Joint Propulsion Conference, Indianapolis, IN, 27–29 June 1994; received 6 August 1994; revision received 6 December 1999; accepted for publication 20 April 2000.

*Manager, Space Communications Advanced Concepts, P.O. Box 3999, M/C 85-13. Associate Fellow AIAA.

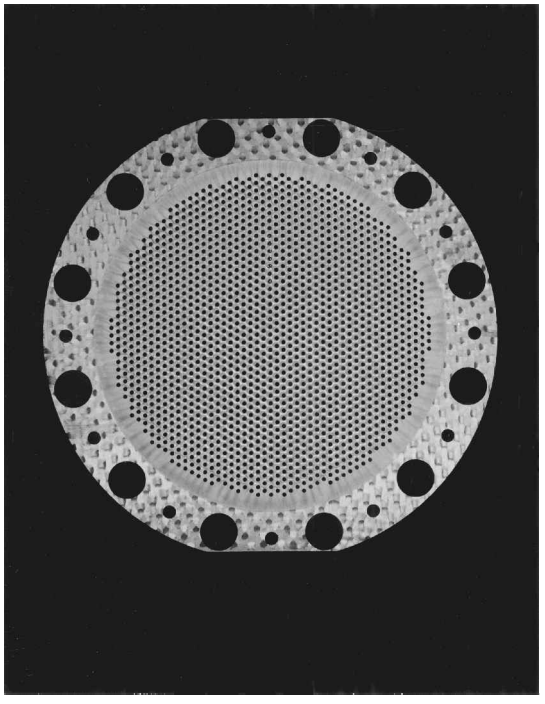

Fig. 1 Carbon–carbon accelerator grid.

and the spacing in the carbon grids were made to match those of the molybdenum grids closely.

Carbon–Carbon Grids

The carbon grids were fabricated from flat panels 0.9 mm thick made of three plies of five-harness satin weave fabric laid up in a [0, 45, 0] orientation. The fabric contained pitch-based fiber 10 μm in diameter, and the fiber modulus was 7.2×10^{11} Pa. The matrix was pure carbon suffused into the fabric by chemical vapor infiltration. The coefficient of thermal expansion of these panels ranged from -2.0×10^{-6}/K at 295 K to about $+1.0 \times 10^{-6}$/K at 675 K. The density was 1.65 g/cm^3.

With a 1.5-kW CO_2 laser, we machined the panels into circular grids comprising a 9.6-cm-diam array of circular apertures. The laser cutting of the apertures produced conical holes with a straight 6-deg taper. The two grids were installed so that the narrow ends of the holes faced together. We sanded the screen grid to a thickness of 0.42 mm and the accelerator grid to 0.51 mm. The screen grid had not previously been used, but the accelerator grid was the same one used in the previous wear tests and was resanded slightly to recreate a smooth, uneroded downstream surface. Figure 1 shows the downstream side of the accelerator grid.

Molybdenum Grids

The apertures in the molybdenum grids were chemically milled. These grids were dished inward (into the thruster discharge chamber), and the aperture positions in the accelerator grid were adjusted to compensate for the dished shape. As with the carbon grids, to start the new test with a smooth surface on the downstream side of the accelerator grid we polished away the erosion depressions created during the previous tests.

The grid mount used for both the carbon and the molybdenum grids was a pair of molybdenum rings designed specifically for the molybdenum grids. They worked well at maintaining good grid alignment with the molybdenum grids, but thermal mismatch shifted the alignment of the carbon grids slightly during thermal transients. Table 1 summarizes the characteristics of both grid sets.

Table 1 Carbon and molybdenum grid descriptions

Parameter	Carbon	Molybdenum
Beam diameter, cm	9.6	9.6
Grid profile	Flat	Dished
Hole quantity	1615	1614
Hole spacing, mm	2.29	2.29
Hole profile	Tapered 6 deg	Dual cupped
Screen grid hole diameter, mm	1.78	1.90
Accel grid hole diameter, mm	1.09	1.14
Screen grid open area fraction	0.56	0.63
Accel grid open area fraction	0.21	0.23
Screen grid thickness, mm	0.42	0.36
Accel grid thickness, mm	0.51	0.38
Grid-to-grid gap, mm	0.54	0.60
Accel grid mass, g	9.0	49.0

Apparatus and Test Facility

The ion source used for these tests was a commercial 15-cm-diam discharge chamber with water cooling. An adapter masked the chamber exit down to 10 cm and provided an attachment for the 10-cm molybdenum grid mount. The cathode and neutralizer for this ion source were tungsten filaments. To avoid tungsten deposition on the downstream side of the accelerator grid, the neutralizer was removed.

The test facility was a 5.5-m-high $\times$ 2.4-m-diam vacuum chamber pumped by three 1.2-m helium cryopumps. With all three pumps operating, the pumping speed was 79,000 l/s on xenon, which produced a background pressure of 1×10^{-4} Pa for the current tests. Part of the time only two pumps were operating because of difficulty with bringing the third pump on line as quickly as the other two. The background pressure during this time was 2.5×10^{-4} Pa. The mounting port for the thruster is at the top of the chamber, and the thruster beam was directed vertically downward at the bottom of the chamber. The length of the chamber is sufficient to preclude significant deposition on the thruster of backscattered material from the chamber bottom and walls.

Mass spectrometer measurements of the constituents of the gas supplied to the thruster by the xenon feedline revealed that a small but significant amount of air had been leaking into the line. In our initial erosion tests referred to in the Introduction, a possible cause of the unexpectedly high carbon erosion rate was excessive presence of oxygen, water vapor, and nitrogen. Each of these react with carbon to form volatile compounds that evaporate from the carbon surface, whereas the compounds that molybdenum forms with nitrogen and oxygen are solids that remain on the surface and reduce the rate of erosion. The impact of charge-exchange ions could provide the activation energy for the reactions, so that with the carbon grids the mass loss due to chemical reaction would occur just where erosion by charge-exchange ions occurs. The background nitrogen partial pressure in the test chamber during the original tests was measured to be 3×10^{-5} Pa, about half of the threshold value at which the erosion of molybdenum is known to be affected by the formation of passivating nitrogen compounds. It is possible, though, that sufficient air was getting into the propellant flow line to raise the nitrogen partial pressure above the threshold level in the vicinity of the thruster exit.

The xenon feedsystem was rebuilt for the current test to minimize the amount of air and water vapor present in the propellant gas. We configured the new system so that the flow-control needle valve was located inside the vacuum chamber so that the portion of the line outside the chamber had an internal pressure above ambient to avoid air permeation into the line. The line was stainless steel tubing 6 mm in diameter. The total length was less than 2 m, with about 1 m of it outside the chamber. It was not electropolished, but we baked it out until the concentration of water vapor in the xenon flow was less than 1 ppm at a xenon flow rate of 3 mg/s, about 10 times the flow rate used during the grid tests.

The instrument used to measure the depth of the erosion on the grids was a laser profilometer with a vertical resolution of 0.4 μm, and the horizontal sampling interval was 15.24 μm. The masses of the grids before and after the tests were measured with an electronic scale accurate to 0.1 mg.

Procedure

Before the tests we measured the surface profiles between several pairs of holes at the centers of the carbon and the molybdenum

Table 2 Thruster operating conditions

Parameter	Value
Beam voltage, V	600
Accelerator grid voltage, V	−300
Discharge voltage, V	35
Xenon flowrate, mg/s	0.29
Beam current, mA	80
Propellant utilization	0.37
Chamber pressure (corrected for Xe), Pa	1.3×10^{-4}
Accelerator grid current (estimate), mA	0.3–0.4

accelerator grids to provide baselines for the posttest measurements. We also weighed the two grids after baking them for three days at 200°C to dry them fully. The baking proved to be important only for the carbon grid.

Before putting the carbon grid set under vacuum, we applied a voltage across the grids just high enough to cause a steady rate of arcing in air. Sustaining this condition for a while served to clear away loose carbon fibers that on earlier occasions had caused an unclearable short in the vacuum.

We operated this grid set for 420 h. The test was intended to be continuous except for a planned shutdown for replacing the filament cathode, but three other inadvertent interruptions occurred, all before the planned shutdown. One was due to a power outage, and two others were shutdowns to recycle the experiment control software. In these three instances, the test chamber remained under vacuum and the beam source was off for $\frac{1}{2}$ h or less. Nevertheless, after each one the accelerator grid current measurement showed a step increase of slightly more than 0.1 mA, apparently caused by thermally induced shifts in the grid alignment. These increases totaled 0.4 mA. The test interruptions occurred at 60, 110, and 149 h into the test. At 240 h, the cathode was replaced and the grids realigned. The accumulated operating time with grid misalignment thus totaled 180 h. The remaining 180 h of the test ran without further interruption. Subsequently, the molybdenum grids were tested for 225 h, with one interruption to replace the xenon supply tank. No alignment shifting occurred with these grids.

Table 2 lists the nominal operating conditions of the thruster for the two tests. Automatic regulation of the cathode current maintained the beam current at the setpoint ±1%. This ensured that the beam density and, hence, the rate of production of charge-exchange ions, was the same for the two tests.

The accelerator grid current could not be determined precisely, because we found that the grid insulators gradually became slightly conductive. The conductivity was temperature dependent and appeared to be essentially zero when the beam source was first started, and so the accelerator grid current at that time was taken to be the impingement current.

After the tests, we reweighed and rescanned the accelerator grids. The tungsten filament cathode caused some tungsten to deposit on them on the upstream side. With the carbon grid we could remove this without affecting the grid by immersing the grid alternately in sodium hydroxide and nitric acid for brief periods. A test with a control coupon of the same carbon–carbon material verified that this treatment did not also remove some carbon. We reweighed the grid to determine the tungsten deposition and the final mass of the grid (the grid was baked dry prior to each weighing). The amount of tungsten deposited on the molybdenum grid was assumed to be in proportion to the operating time relative to the operating time of the carbon grid.

Results

Carbon–Carbon Grids

Figure 2 shows the center of the accelerator grid at 15 times magnification as it appeared after 420 h of operation. The labels A, B, C, and D mark the four holes that were the endpoints of surface scans made with the profilometer. Although erosion may not be apparent in the reproduction here, the photograph original faintly shows a typical hexagonal erosion pattern. The erosion was so slight it was not discernable in direct viewing by eye. The photograph

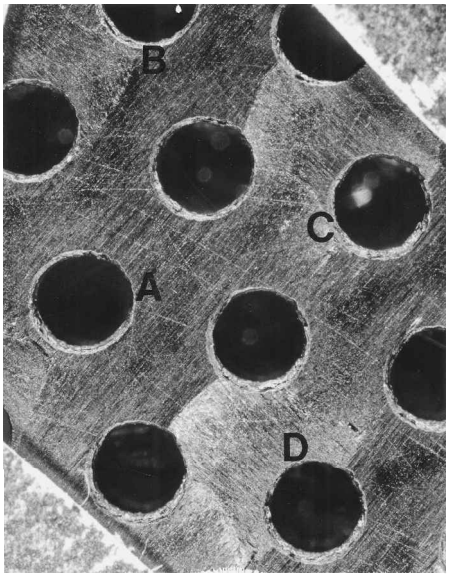

Fig. 2 Center of the carbon grid after 420 h of operation.

shows the erosion pattern to be shifted slightly, directly upwards in the photograph, from the centered, symmetrical position expected if the screen and accelerator grids were precisely aligned. The weave of the carbon-fiber fabric is apparent, and scratch marks remain evident from the sanding done before the test.

Figure 3 shows three of the surface profiles measured before the erosion test. Figure 4 shows posttest profiles made from A to C, C to B, and B to A. Along each of these, at least one erosion depression is evident, and along B to A possibly a second one is discernable. There ought to be two erosion depressions along all of the paths, but because the erosion was not visible the profilometer could not be aimed specifically to traverse the depressions. In an attempt to find the desired paths, we made multiple parallel passes, spaced 0.12 mm apart, between the three pairs of holes represented in Fig. 4. The profiles in Fig. 4 are the best obtained. Just one path was taken each from A to D and D to C, and apparently neither passed where measurable erosion had occurred. Along A to C and C to B, the depressions are centered at 1.8 and 0.7 mm along the profiles, respectively, and are 2.1 and 2.5 μm deep as measured on the smoothed profiles in Fig. 4b. The two depressions along B to A are at similar locations and are 3.0 and 2.0 μm deep. The deeper one occurs at the location of one of the most distinct spots of erosion on the photograph. This spot overlaps a boundary between two sections of fabric that corresponds to the abrupt edge depicted in the profile. Along A to C, the narrow pit at 0.8 mm appears to have been a preexisting surface feature. It is located where the photograph shows a pair of scratches crossing each other in the erosion trough between two of the depressions.

The mean depth of the four measurable erosion depressions is 2.4 μm. The maximum likelihood value for the standard deviation of the mean is 0.23 μm (this is the sample standard deviation divided by the square root of the number of measurements in the sample).

We were unable to determine the mass loss caused by charge-exchange ions. The measured reduction in mass was 35 ± 5 mg (0.4% of the total grid mass), after removal of 18 mg of tungsten deposition. This is many times any realistic estimate of the mass that might have been eroded by charge-exchange ions. At least a third of the mass loss could reasonably have been caused by direct-impingement erosion resulting from grid misalignment after the three unplanned test interruptions. The total amount of direct impingement was roughly 60 mA-h. Also, the pretest process of subjecting the grids to arcing in air burned away some material.

Molybdenum Grids

After 225 h of operation, the molybdenum accelerator grid exhibited a well-defined hexagonal erosion pattern, as Fig. 5 shows.

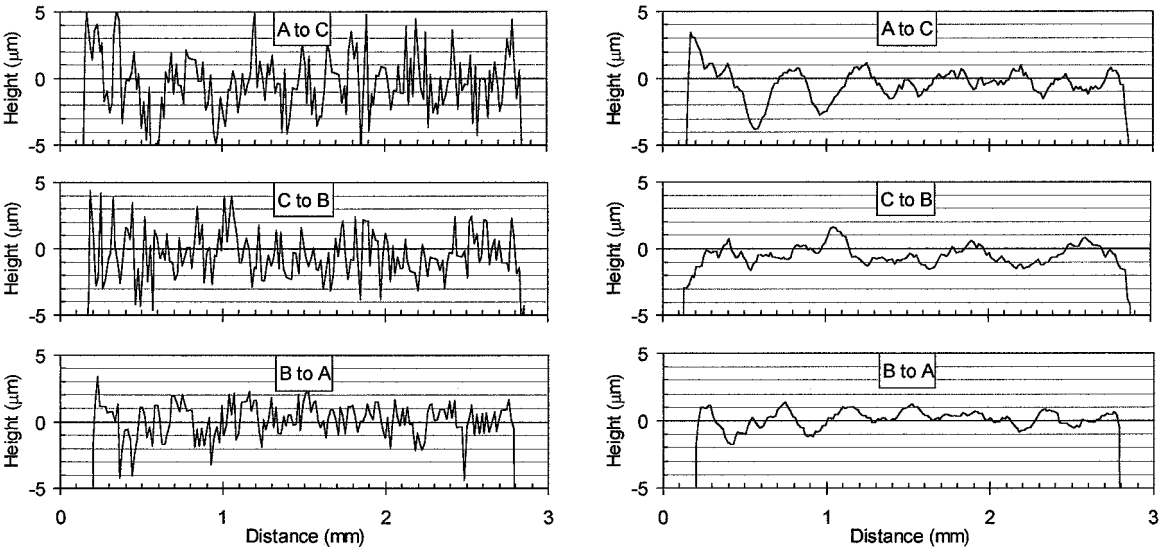

a) As measured b) Smoothed (nine-point moving average)

Fig. 3 Pretest surface profiles from the carbon accelerator grid.

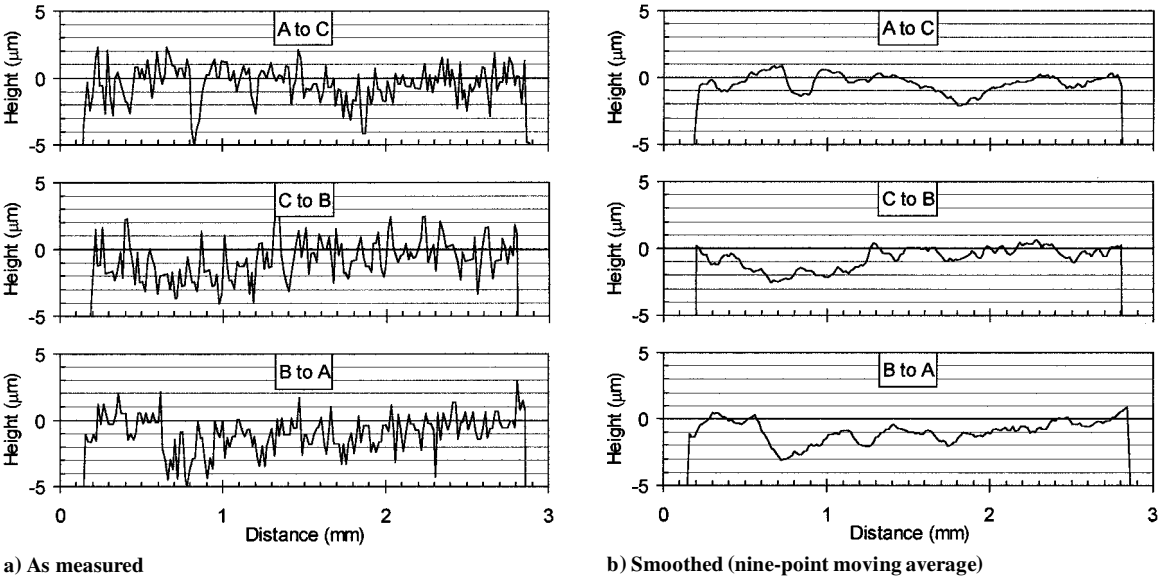

a) As measured b) Smoothed (nine-point moving average)

Fig. 4 Posttest surface profiles from the carbon accelerator grid.

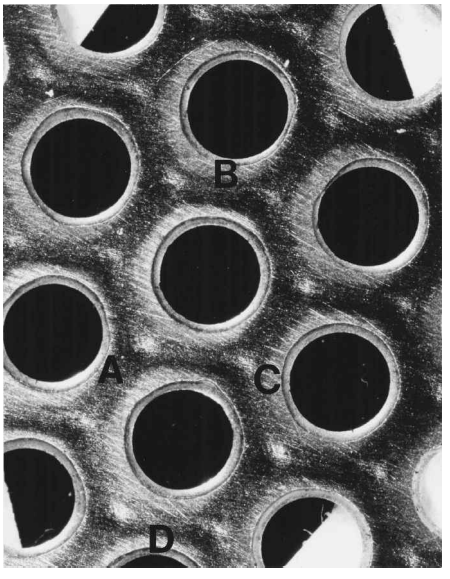

Fig. 5 Center of the molybdenum grid after 225 h of operation.

This pattern was also shifted slightly, in this case downward and to the left. The lighting in the photograph makes the eroded areas appear mostly dark, although they are actually as shiny as the uneroded surface close around each hole. Note that the cupped shape of the holes (caused by the chemical milling) makes them appear stepped. As with the carbon grid, profilometer scans were made along lines between the labeled holes. Only a single profile was taken between each pair of holes.

Figure 6 shows representative surface profiles. The posttest profiles each depict a pair of pronounced erosion pits. The D-to-C profile, in particular, appears to have captured the pit centers, or very nearly so. As determined from Fig. 6b, the pit depths are 21.5 and 19.8 μm and the trough connecting the pits is 6 μm deep. Along C to B the recorded depth of one pit is only 14.5 μm and of the other is 20.8 μm. It is likely that the scan passed over the sidewall of one pit, skimmed at a slight angle along the side of the trough, and passed near the center of the second pit. The other three profiles show pit depths between the shallowest and deepest shown here, as listed in Table 3. The mean depth of the pits is 18.1 μm. The standard deviation of the mean is 0.85 μm.

The mass loss due to erosion during the test was 125 ± 3 mg, after adjustment for an estimated 10 mg of deposition of tungsten on the upstream side of the grid. This is 0.3% of the total grid mass of

49 g. The density of molybdenum is 10.2 g/cm^3, and so the volume eroded was 1.2 mm^3.

Discussion

The lack of a means to determine the carbon mass loss due specifically to erosion by charge-exchange ions prevents direct comparison of the total amounts of erosion from the two accelerator grids. An alternative approach is to compare the mean depths of the erosion pits at the centers of the two grids.

Carbon Grid Set Operating Time

A factor to account for in making this comparison arises from the alignment shifts that occurred during the interruptions in the test of the carbon grid set. Following each restart, the erosion would have been displaced from its earlier location, causing the erosion depressions to broaden more than deepen. (Broadening was clearly evident in the surface profiles measured in our earlier tests, in which the carbon grid set became misaligned also.) Furthermore, it is not known how precisely the realignment done at 240 h coincided with the initial alignment. The longest time of continuous operation in one position was the 180 h following the realignment and lasting until the end of the test. For the purpose at hand, it appears that the best way to quantify the cumulative effect of the other blocks of time is to treat them as random variables with uniform probability distributions. In particular, the 60 h at the start of the test could have produced erosion entirely coincident with that of the final 180 h, or it could, at the other extreme, have produced no significant erosion at all at the places that became the centers of the depressions created in the final 180 h. With no knowledge other than this, it is appropriate to assign a uniform probability distribution across the 60 h. The mean value is then 30 h, and the standard deviation is 17 h. For the period of time when direct grid impingement was occurring, it is certain that the pattern of maximum erosion was not coincident with that of the final 180 h. Some of the erosion could nonetheless have been measurably additive. Absent a firmer estimate, a reasonable supposition is that this period, taken as a single block of 180 h, was at most 50% effective in eroding the places later to become the erosion depressions. At the least it might have produced no additive erosion at all. The mean value for this block then is 45 h, and the standard deviation is 26 h.

Table 3 Summary of depth measurements

Path	Molybdenum, μm		Carbon–Carbon, μm	
A to C	15.4	15.5	—	2.1
C to B	14.7	21.0	2.5	—
B to A	18.1	15.1	3.0	2.0
A to D	19.5	20.4	—	—
D to C	21.5	19.8	—	—
Mean depth	18.1		2.4	
Standard deviation	2.68		0.45	
Normalized standard deviation	15%		19%	
Standard deviation of mean	0.85		0.23	

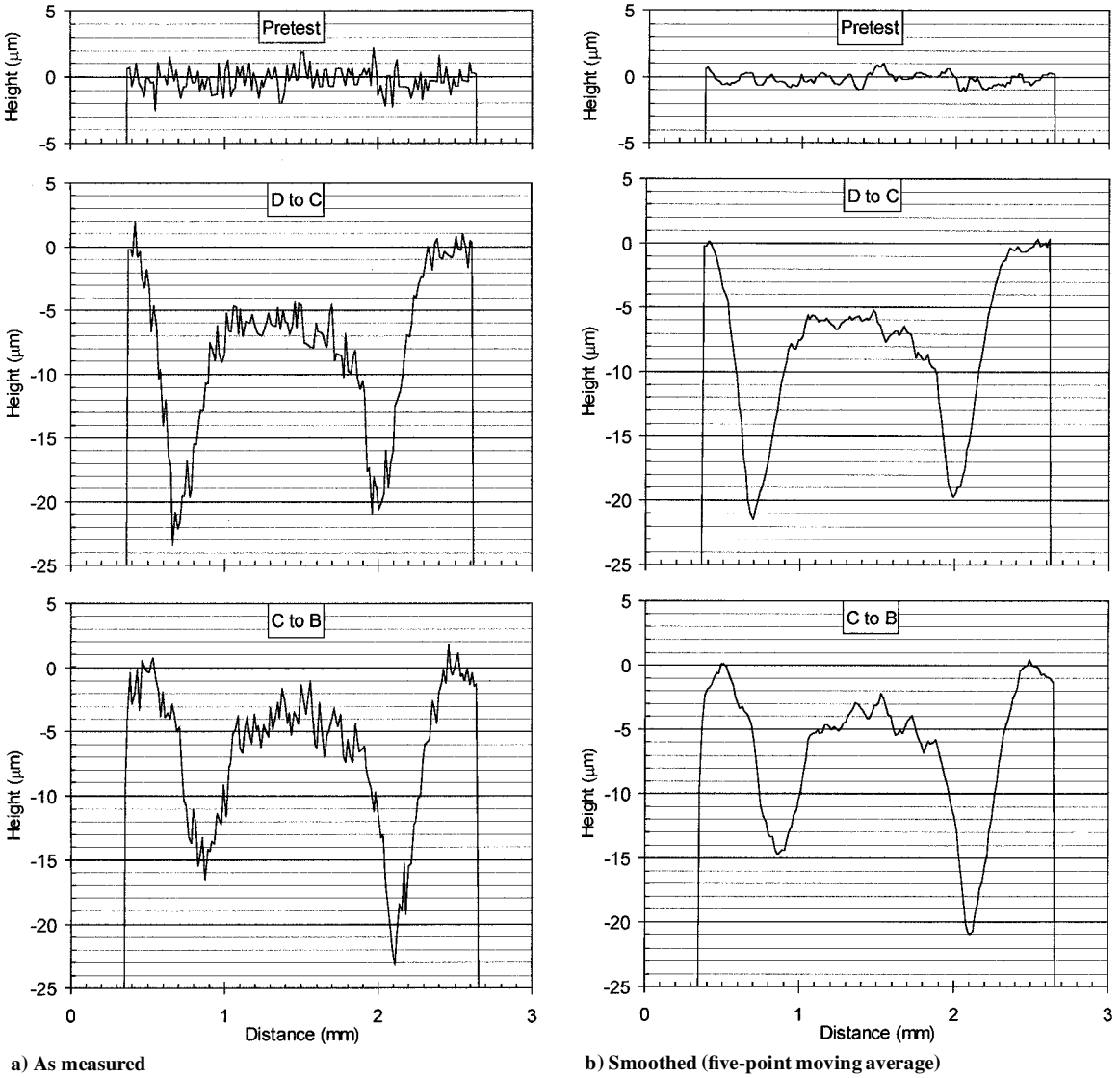

a) As measured b) Smoothed (five-point moving average)

Fig. 6 Surface profiles from the molybdenum accelerator grid; curvature has been subtracted out.

The sum of the three blocks of operating time has a mean value of 255 h. The standard deviation is 31 h, or 12%. Dividing 255 h by 225 h, the operating time of the molybdenum grids, yields 1.13 as the ratio of operating times. The uncertainties in controlling the beam current, neutral flow, operating time, and so on are all negligible in this context; thus, the standard deviation for this ratio is 12%.

Prediction

Measurements by Wehner[17] and Rosenberg and Wehner[18] indicate the sputter yields of molybdenum and carbon are 0.51 and 0.08 atom/ion, respectively, under the impact of 300-eV xenon ions. Assume for the moment that for an accelerator grid voltage of −300 V all of the charge-exchange ions striking the accelerator grid do so with an energy of 300 eV. Then the rate at which atoms are sputtered off should be 6.4 times as much with molybdenum as it is with carbon. The ratio of the atomic masses of molybdenum (95.94 amu) and carbon (12.01 amu) is 7.9, making the expected mass loss rate of carbon only $\frac{1}{50}$ that of molybdenum. The ratio of the density of molybdenum, 10.2 g/cm^3, to the density of the carbon–carbon composite panels the carbon grids were made of, 1.65 g/cm^3, is 6.2. Hence, on a volumetric, or depth, basis the ratio of the erosion rates of the carbon and molybdenum accelerator grids would be 1:8.2.

Recently, Blandino et al.[19] directly measured the relative erosion rates of carbon–carbon and molybdenum test coupons to be 1:7.3 and 1:7.7 at xenon ion energies of 500 and 750 eV, respectively. The Wehner[17] and Rosenberg and Wehner[18] sputter data for 500-eV xenon impacts are 0.90 atom/ion for molybdenum and 0.17 atom/ion for carbon, giving a ratio of 5.3, nearly 20% smaller than at 300 eV. For comparison to the Blandino et al.[19] data, this would imply a relative erosion rate of 1:6.8 for our first-generation carbon–carbon panels, which had a somewhat lower density than is typical of newer material Blandino is likely to have used.

The average impact energy, however, of the charge-exchange ions created in the exit region of an ion thruster is less than the accelerator grid potential. Many of the ions are produced upstream of the charge neutralization, or zero potential, plane and, thus, do not have the full grid potential to fall through as they are drawn back to the grid. As indicated by the data just cited, the sputter yield for carbon declines more rapidly than that for molybdenum when the ion impact energy is reduced. At 200 eV, the sputter yields measured by Wehner[18] are 0.28 and 0.04 atom/ion for molybdenum and carbon, respectively. The ratio between them is 10% higher than at 300 eV. If one assumes an effective average impact energy of 200 eV, the predicted relative erosion of the carbon and molybdenum accelerator grids is 1:9.0. One would then expect the overall erosion ratio to tend toward one-ninth, while the ratio of the pit depths would likely be closer to one-eighth. The pits are formed where the electric field focuses the charge-exchange ions produced farthest from the grid, those that strike at the full potential of 300 V.

Measurement

It is not assured that the measurements in Figs. 4 and 6 all passed through the deepest part of each erosion pit shown, and so the data will not provide a direct comparison of the pit depths in the two grids. At best, it can only be assumed that the sample averages for the carbon and the molybdenum are both biased below the actual average pit depths by the same percentage. The similar magnitudes of the normalized sample standard deviations (see Table 3) support this assumption. (The normalized standard deviation for the carbon data is somewhat larger, as would be expected because other factors are more pronounced due to the much smaller mean depth and the greater surface roughness.)

The ratio of the mean depths of the recorded pits on the molybdenum and carbon grids is 1:7.5, and adjusting this by the operating-time ratio yields 1:8.5, consistent with the prediction. Also, the ratio of the maximum recorded pit depths from each grid is 1:8.1 after we factor by the operating-time ratio, which lends additional support to this result. This accords with the argument that at the pit centers the erosion rates should correspond to greater ion impact energy.

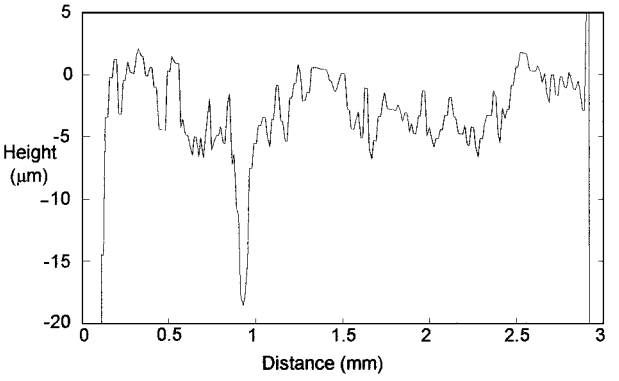

Fig. 7 Posttest carbon-grid surface profile from the previous erosion test.

Considerable uncertainty accompanies this end result, due to the substantial magnitudes of the standard deviations of the three principal random variables in the data analysis: the sample means and the operating-time ratio. The aggregate standard deviation is approximately 16%. This value is the square root of the sum of the squares of the normalized standard deviations of those variables.

Of more interest is the usual two-sigma (that is, two standard deviation) error band. Equivalently, for a normal distribution, this is the 95% confidence interval. For the three principal random variables, there are three different 95% confidence intervals. For the carbon sample mean it is ±3.3 sigma (t distribution with three degrees of freedom), for the molybdenum sample mean it is ±2.3 sigma (t distribution with nine degrees of freedom), and for the operating-time ratio it is about ±1.8 sigma (combination of two uniform distributions). The weighted average of these is 2.5 sigma, using the variances of the three variables as the weights. This multiplied by the one-sigma value of 16% yields ±40% as the approximate 95% confidence interval. The error band for the calculated ratio of erosion rates thus spans approximately from $\frac{1}{6}$ to $\frac{1}{14}$.

Previous Results

As noted, our previous tests had yielded a carbon/molybdenum erosion ratio of one-third.[15] If the carbon erosion rate observed then had persisted in the current tests, after 240 h the erosion depressions would have been nearly 10 μm deep and, after 420 h, more than 15 μm deep. After the previous tests there were locations where narrow cavities penetrated several times deeper than the erosion pits within which they were located. Figure 7 is a surface profile from the previous test showing one such cavity. The locations of the cavities coincided with places in the carbon fabric weave where there had been gaps between the fibers that exposed some low-density graphite matrix to the impacting ions. This time there was no evidence of such cavities. The difference in test conditions between the previous test and the current one has clearly altered the erosion process. The changes in the conditions were the near elimination of air permeation into the xenon feedline and the reduction of the background pressure in the test chamber. This reduced to insignificant levels the concentrations of oxygen, water vapor, and nitrogen available to react with the carbon at the ion impact sites. With little doubt, therefore, the presence of these contaminants was the reason for the high carbon erosion rate that occurred in the earlier test.

Similarly, at the erosion rate previously experienced with the molybdenum grids, the erosion depressions this time would have been 25 μm deep. Some nitrogen passivation of the molybdenum surface probably occurred in the earlier test.

Future Improvements

Improvements in fabrication methods will produce carbon–carbon grids with a density of 1.9 g/cm^3 or better, 20% more than the density of our prototypes, and with a more extensively ordered graphitic matrix. Both of these factors will reduce the amount of surface regression resulting from charge-exchange erosion. In addition, tailored design approaches appropriate to carbon–carbon material

enable making the accelerator grid thicker where the erosion is most severe, without reducing the ion optics perveance. Then carbon grids could be capable of sustaining more than 10 times the total charge-exchange ion flux that molybdenum grids can.

Conclusion

In a pair of comparative wear tests, we operated a prototype carbon–carbon grid set and a conventional molybdenum grid set under similar conditions for 420 and 225 h, respectively. The surface regression measured on the downstream sides of the accelerator grids indicated that the rate of erosion on the carbon grid was as predicted: midway between $\frac{1}{8}$ and $\frac{1}{9}$ of the erosion rate on the molybdenum grid. The error band for this result is relatively wide, from $\frac{1}{6}$ to $\frac{1}{14}$, due to consequences of shifts in the alignment of the carbon grid set. Therefore, we can only tentatively conclude that carbon–carbon grids will exhibit the high degree of erosion resistance expected. Additional sustained testing is necessary to confirm this fully.

Effort taken to prevent air seepage into the xenon feedline, plus operation at low background pressure, avoided recurrence of the rapid carbon erosion observed previously. This difference in results confirms that the presence of oxygen, nitrogen, and water vapor in the previous test had accelerated the surface regression rate by as much as a factor of three through chemical reactions with the carbon.

Improved processes and materials that are now available for use in making thin carbon–carbon panels will enable fabrication of stiffer, denser, and more erosion-resistant grids than the first prototypes used in this test. The low erosion rate measured in this experiment provides initial confirmation that carbon–carbon grids can enable thrusters to produce a lifetime total impulse of an order of magnitude greater than is possible with molybdenum grids.

Acknowledgments

Michael Rorabaugh contributed immeasurably in the development of the materials and processes used to fabricate the carbon–carbon grids. The author is indebted to Thomas Montgomery for capably conducting the erosion tests and to Patrick Anderson for the profilometer measurements.

References

[1]Patterson, M. J., "Low-Isp Derated Thruster Operation," AIAA Paper 92-3203, July 1992.

[2]Patterson, M. J., Haag, T. W., and Williams, G. J., "Derated Ion Thruster Development Status," AIAA Paper 93-2225, July 1993.

[3]Peng, X., Keefer, D., and Ruyten, W. M., "Plasma Particle Simulation of Electrostatic Ion Thrusters," *Journal of Propulsion and Power*, Vol. 8, No. 2, 1992, pp. 361–366.

[4]Peng, X., Ruyten, W. M., and Keefer, D., "Three-Dimensional Particle Simulation of Grid Erosion in Ion Thrusters," Paper IEPC-91-119, *Proceedings of the 22nd International Electric Propulsion Conference*, Oct. 1991.

[5]Peng, X., Ruyten, W. M., and Keefer, D., "Further Study of the Effect of the Downstream Plasma Condition on Accelerator Grid Erosion in an Ion Thruster," AIAA Paper 92-3829, July 1992.

[6]Ruyten, W. M., Friedly, V. J., Peng, X., Celenza, J. A., and Keefer, D., "Spectroscopic Investigations of Beam–Plasma Interactions in an Ion Plume," AIAA Paper 93-1791, June 1993.

[7]Monheiser, J. M., "Development and Verification of a Model to Predict Impingement Currents for Ion Thrusters," NASA CR-195322, April 1994.

[8]Brophy, J. R., Garner, C. E., and Pless, L., "Ion Engine Endurance Testing at High Background Pressures," AIAA Paper 92-3205, July 1992.

[9]Kerslake, W. R., and Pawlik, E. V., "Additional Studies of Screen and Accelerator Grids for Electron-Bombardment Ion Thrusters," NASA TN D-1411, 1963.

[10]Monheiser, J. M., and Wilbur, P. J., "An Experimental Study of Impingement-Ion-Production Mechanisms," AIAA Paper 92-3826, July 1992.

[11]Garner, C. E., and Brophy, J. R., "Fabrication and Testing of Carbon–Carbon Grids for Ion Optics," AIAA Paper 92-3149, July 1992.

[12]Garner, C. E., Brophy, J. R., and Mueller, J., "Fabrication and Testing of 15-cm-dia. Carbon–Carbon Grid," Paper IEPC-93-112, *Proceedings of the 23rd International Electric Propulsion Conference*, Seattle, WA, Sept. 1993.

[13]Mueller, J., Brophy, J. R., and Brown, D. K., "Endurance Testing and Fabrication of Advanced 15-cm and 30-cm Carbon–Carbon Composite Grids," AIAA Paper 95-2660, July 1995.

[14]Hedges, D. E., and Meserole, J. S., "Demonstration and Evaluation of Carbon–Carbon Ion Optics," *Journal of Propulsion and Power*, Vol. 10, No. 2, 1994, pp. 255–261.

[15]Meserole, J. S., and Hedges, D. E., "Comparison of Erosion Rates of Carbon–Carbon and Molybdenum Ion Optics," Paper IEPC-93-111, *Proceedings of the 23rd International Electric Propulsion Conference*, Seattle, WA, Sept. 1993.

[16]Meserole, J. S., "Measurement of Relative Erosion Rates of Carbon–Carbon and Molybdenum Ion Optics," AIAA Paper 94-3119, June 1994.

[17]Wehner, G. K., "The Aspects of Sputtering in Surface Analysis Methods," *Methods of Surface Analysis*, edited by A. W. Czanderna, Elsevier, New York, 1975, p. 10.

[18]Rosenberg, D., and Wehner, G. K., "Sputtering Yields for Low Energy He^+-, Kr^+-, and Xe^+-Ion Bombardment," *Journal of Applied Physics*, Vol. 33, No. 5, 1962, p. 1842,

[19]Blandino, J. J., Goodwin, D. G., Garner, C. E., and Brophy, J. R., "Evaluation and Development of Diamond Grids for Ion Optics," AIAA Paper 95-2663, July 1995.